Linking channel hydrology with riparian wetland accretion in tidal rivers

Scott H. Ensign,[1,2] Gregory B. Noe,[1] and Cliff R. Hupp[1]

Received 22 January 2013; revised 25 November 2013; accepted 26 November 2013; published 14 January 2014.

[1] The hydrologic processes by which tide affects river channel and riparian morphology within the tidal freshwater zone are poorly understood yet are fundamental to predicting the fate of coastal rivers and wetlands as sea level rises. We investigated patterns of sediment accretion in riparian wetlands along the nontidal through oligohaline portion of two coastal plain rivers in Maryland, U.S., and how flow velocity, water level, and suspended sediment concentration (SSC) in the channel may have contributed to those patterns. Sediment accretion was measured over a 1 year period using artificial marker horizons, channel hydrology was measured over a 1 month period using acoustic Doppler current profilers, and SSC was predicted from acoustic backscatter. Riparian sediment accretion was lowest at the nontidal sites (mean and standard deviation = 8 ± 8 mm yr^{-1}), highest at the upstream tidal freshwater forested wetlands (TFFW) (33 ± 28 mm yr^{-1}), low at the midstream TFFW (12 ± 9 mm yr^{-1}), and high at the oligohaline (fresh-to-brackish) marshes (19 ± 8 mm yr^{-1}). Channel maximum flood and ebb velocity was twofold faster at the oligohaline than tidal freshwater zone on both tidal rivers, corresponding with the differences in in-channel SSC: The oligohaline zone's SSC was more than double the tidal freshwater zone's and was greater than historical SSC at the nontidal gages. The tidal wave characteristics differed between rivers, leading to significantly greater in-channel SSC during floodplain inundation in the weakly convergent than the strongly convergent tidal river. High sediment accretion at the upstream TFFW was likely due to high river discharge following a hurricane.

Citation: Ensign, S. H., G. B. Noe, and C. R. Hupp (2014), Linking channel hydrology with riparian wetland accretion in tidal rivers, *J. Geophys. Res. Earth Surf.*, *119*, 28–44, doi:10.1002/2013JF002737.

1. Introduction

[2] Tidal freshwater rivers exist at the interface between fluvial and estuarine systems. A tidal freshwater river channel and its adjoining wetlands form an interacting biogeomorphic system of sediment and water exchange (hereafter we refer to this system as a tidal river). Fluvial and estuarine processes overlap within the tidal river and considerable research has been devoted to examining the geomorphology of tidal river channels (reviewed by *Dalrymple and Choi* [2007] and *Hughes* [2012]) and tidal freshwater wetlands (reviewed by *Conner et al.* [2009] and *Barendregt et al.* [2009]). Tidal rivers cross through a critical transition zone (sensu *Phillips and Slattery* [2008]) on the coastal plain in which profound changes in sediment storage and flux occur. Further research on these processes is needed to explain the formation and maintenance of tidal river landforms, particularly near the limit of tidal influence where tides have only just begun to affect river and wetland processes. An important application of these efforts is to more accurately predict how sea level rise in the coming decades will alter and extend the spatial distribution and characteristics of tidal river channels and intertidal wetlands.

[3] A defining characteristic of tidal rivers is that sediment transport in the channel and wetlands is influenced by tidal flow far upstream from the limit of saline water. Sediment from the saline estuary can be transported into the freshwater river by asynchrony between flood and ebb flow velocity [*Friedrichs and Aubrey*, 1988]. This tidal asynchrony leads to tidal pumping which can drive net upstream transport of suspended [*Guézennec et al.*, 1999; *Chen et al.*, 2005] and bed sediments [*Ashley*, 1980] into the tidal freshwater zone. Remarkably, some of the material that contributes to freshwater wetland accretion can be of marine origin [*Schuchardt and Schirmer*, 1990]. Watershed processes also exert significant influence on tidal river geomorphology [*Khan and Brush*, 1994; *Hilgartner and Brush*, 2006], and a central challenge in tidal river research is parsing the influence of watershed floods from tides on sediment flux and wetland accretion [*Phillips*, 1997].

[1]National Research Program, U.S. Geological Survey, Reston, Virginia, USA.
[2]Aquatic Analysis and Consulting, LLC, Morehead City, North Carolina, USA.

Corresponding author: S. H. Ensign, Aquatic Analysis and Consulting, LLC, 603 Mandy Court, Morehead City, NC 28557, USA. (scott@aquaco.us)

©2013. American Geophysical Union. All Rights Reserved.
2169-9003/14/10.1002/2013JF002737

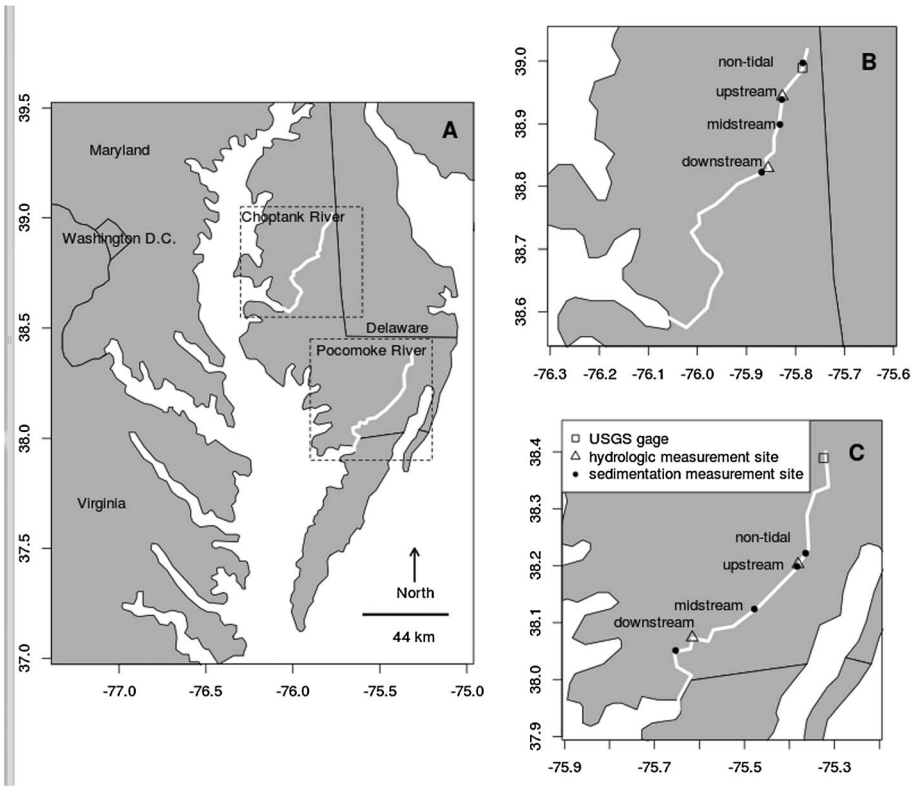

Figure 1. Location of the (a) Choptank and Pocomoke Rivers with respect to the Chesapeake Bay and the nontidal (USGS stream gaging network), tidal flow gages (this study), and floodplain sediment accretion sites on the (b) Choptank and (c) Pocomoke.

[4] Patterns of in-channel sediment transport affect patterns in sediment accretion in tidal river wetlands. Sediment accretion in tidal river wetlands has been found to increase with proximity to the estuarine turbidity maximum (ETM) [*Darke and Megonigal*, 2003]. This downstream increase in sediment accretion is not solely a function of sediment concentration in flood water but also is dependent on the influence of wetland vegetation that slows flow and induces deposition of this sediment [*Leonard*, 1997; *Leonard and Reed*, 2002]. Tidal wetlands near the ETM include emergent tidal freshwater and oligohaline marshes, but the majority of tidal river freshwater wetlands are forested [*Field et al.*, 1991; *Conner et al.*, 2009]. Tidal freshwater forested wetlands (TFFW) have relatively low rates of sediment accretion [*Baldwin*, 2009; *Craft*, 2012; *Ensign et al.*, 2013b] and are at substantial risk of habitat change as sea level rise changes their hydrology and salinity [*Yanosky et al.*, 1995; *Krauss et al.*, 2009; *Cormier et al.*, 2012]. It is unclear why TFFW accretion rate is uniformly low across a range of rivers with widely varying suspended sediment regimes. It also is unknown how accretion changes between the nontidal river and tidal river and estuary, and whether differences in accretion occur within the zone of TFFW.

[5] Channel sedimentation and floodplain accretion ultimately affect tidal dynamics. Tidal waves become deformed as they travel through tidal channels and wetlands, and the resulting asymmetry between ebb and flood velocity affects the predominant direction of sediment transport [*Friedrichs and Aubrey*, 1988; *Savenije*, 2005]. This deformation also affects the relationship between tide stage and flow direction: Tidal channels that are long, deep, and lack strong convergence of channel cross section (the rate at which cross section decreases with distance upstream from the river mouth) exhibit tides with progressive wave characteristics (high and low water levels occur at maximum flow velocity) [*Savenije*, 2005]. In contrast, tidal channels that are short (less than 1 quarter the tidal wavelength) and shallow exhibit tides which are more characteristic of standing waves (high and low water levels occur at zero flow velocity). The degree to which a channel's tidal wave is progressive or standing can be quantified by the length in the phase lag between high water and high water slack current flow and low water and low water slack current flow [*Savenije*, 2005]. For example, *Yankovsky et al.* [2012] examined phase lags and the M_2:M_4 tidal harmonics in at tidal freshwater river channel and found strong flood dominant tidal asymmetry. These tidal wave characteristics are reflected in distinct hysteresis patterns in stage and velocity that are affected by tidal channel and wetland morphology [*Pethick*, 1980; reviewed by *Hughes*, 2012].

[6] The contrast between progressive and standing tidal waveforms may be related to a contrast in channel morphology, with "funnel-shaped", strongly convergent tidal rivers at one end of a spectrum and weakly convergent, meandering tidal rivers at the other [*Wright et al.*, 1973]. Along the tidal freshwater zone, some rivers exhibit a continuous increase in channel width while others exhibit an abrupt increase in width at the nontidal/tidal boundary but maintain a consistent width downstream from that transition. The strongly convergent and weakly convergent tidal rivers studied by *Wright et al.* [1973] exhibited standing and progressive tidal waves,

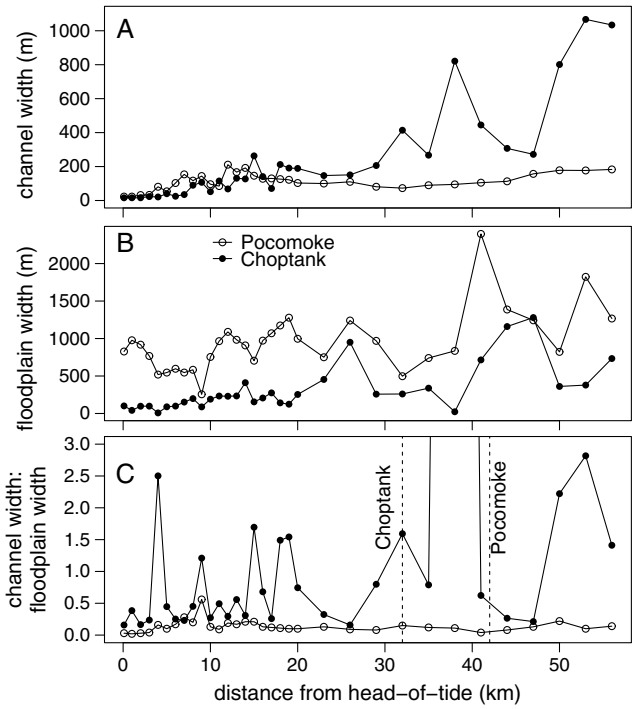

Figure 2. (a) Channel width, (b) floodplain width, and (c) channel to floodplain width ratio on the Choptank and Pocomoke Rivers. Measurements of channel width (vegetated bank to vegetated bank) were made using aerial photographs available on The National Map (www.nationalmap.gov). Floodplain width was measured from U.S. Geological Survey digital topographic maps; distances were measured perpendicular to the river channel and extending to the first 1.5 m contour lines. Vertical dashed lines in Figure 2c indicate the downstream extent of floodplain sampling in the current study.

respectively; the authors suggested that these waveforms were a function of channel morphology. Yet if channel morphology affects waveforms and waveforms affect sediment transport and channel morphology, then self-reinforcing feedback may occur in tidal channels [*Friedrichs and Aubrey*, 1988; *Yankovsky et al*., 2012].

[7] The potential for tidal river morphology to affect tidal waveform and for tidal waveform to affect river morphology in a feedback loop leads to two hypotheses. First, we would expect strongly convergent tidal rivers to exhibit a tide with standing wave characteristics and weakly convergent tidal rivers to exhibit a tide with progressive wave characteristics. Second, with the assumption that suspended sediment concentration (SSC) is proportional to flow velocity, we would expect that rivers with standing tidal wave characteristics would have lower riparian sediment accretion rates because flow velocity (and entrained sediment concentration) would be lowest when the riparian zone was inundated. Furthermore, weakly convergent tidal rivers with progressive wave characteristics would be expected to have higher riparian sediment accretion rates because flow velocity (and SSC) is greater when the riparian zone is inundated.

[8] This study examined these hypotheses along the nontidal through oligohaline portion of two coastal plain rivers with contrasting morphology. In addition, we investigated sediment accretion patterns along the tidal freshwater river. Our study spanned a greater range in riparian sites than have previously been investigated in a single river, including a nontidal floodplain, two TFFW (upstream and downstream), and one oligohaline marsh, thereby allowing a novel comparison between tidal versus nontidal accretion rates. Knowledge of the relative difference in accretion between the nontidal and tidal habitats is necessary to predict how tidal influence will alter riparian sediment accretion as tides extend farther upstream as sea level rises.

2. Methods

2.1. Study Sites

[9] We choose two rivers with similar watershed size and land cover characteristics but contrasting river morphology. The Choptank River drains a 2059 km^2 watershed with land use dominated by agriculture (49%), followed by forest (22%), and wetland (11%) [*Vogelmann et al*., 1998], while the Pocomoke River drains a 2105 km^2 watershed dominated by forest (48%), agriculture (34%), and wetland (14%) [*Cronin*, 2004]. Both watersheds drain the Delmarva Peninsula in Maryland and Delaware, U.S. (Figure 1), whose surficial geology is the result of Pleistocene transgressive-regressive sea level oscillations that sequentially capped the middle and lower peninsula with marine-estuarine deposits forming a series of terraces [*Owens and Denny*, 1979; *Hobbs*, 2004]. Fluvial incision through these deposits and underlying Miocene-Pliocene formations (Pensauken and Beaverdam) and subsequent backfilling of the Choptank and Pocomoke stream valleys has occurred repeatedly throughout the Pleistocene. The Holocene transgression has filled the stream valleys with wetlands overlying the Upper Pleistocene Parsonsburg Sand, whose eolian topographic features (upland dunes and braided stream channels) are still apparent on the landscape [*Newell and Dejong*, 2011].

[10] Morphologically, the two rivers differ in the increase in channel width downstream of the nontidal/tidal boundary. Width of the Choptank River channel increases from 16 m to 206 m over a 29 km length of its tidal freshwater zone, and its sinuosity is 1.18 (Figure 2). The convergence length of the Choptank River from the mesohaline estuary to the head of tide is 7 km (rapid convergence), and its "funnel-shape parameter" (the ratio of convergence length to the downstream terminal width (sensu *Davies and Woodroffe* [2010])) is 7, indicating a strong funnel shape. The width of the Pocomoke River increases from 23 m to 113 m at the end of its tidal freshwater zone (with a conspicuous maximum at 15 km downstream from the head of tide). The Pocomoke River has a meandering river channel with a sinousity of 1.31. The convergence length of the Pocomoke River is 66 km and its funnel-shape parameter is 434, indicating a minimal funnel shape [*Davies and Woodroffe*, 2010]. The differences in morphology between these rivers are also reflected in the ratio of channel width to floodplain width. The width of the Choptank River channel exceeds the floodplain width at several locations along the tidal freshwater zone, indicating a relatively narrow intertidal zone that potentially constrains lateral channel meandering (Figure 2). In contrast, the Pocomoke River channel: floodplain ratio is generally less than 0.5, demonstrating a channel and floodplain system that can accommodate extensive meandering.

Table 1. Summary of ANOVA Examining the Influence of River (Choptank and Pocomoke) and Site (Non-Tidal, Upstream, Midstream, Downstream) on the Cubed Root of Sediment Accretion (mm yr^{-1})

Model	Term	df	*F*
accretion ~ river × site			
	river	1	27.4
	site	3	13.5
	river × site	3	5.5

[11] This study focused on the nontidal through oligohaline portion of each river. Floodplain sediment accretion was measured at four sites on each river (Figure 1). On the Choptank River, TFFW sites were located 10 km ("upstream") and 16 km ("midstream") from the nontidal site located near the limit of tides ("nontidal"), and an oligohaline marsh site ("downstream") was located 28 km downstream from the nontidal site. On the Pocomoke River, TFFW sites were located 5 km ("upstream") and 19 km ("midstream") from the nontidal site, and an oligohaline marsh site ("downstream") was located 42 km downstream of the nontidal site.

[12] Hydrology was investigated at two sites on each river (Figure 1). The sites on the Choptank River were located 9 km ("tidal freshwater zone") and 27 km ("oligohaline zone") downstream from the nontidal floodplain site, while the Pocomoke River sites were located 4 km ("tidal freshwater zone") and 36 km ("oligohaline zone") downstream from the nontidal floodplain site. Hydrology measurement sites were chosen along linear channel reaches (not meander bends) where possible to minimize lateral variations in flow and sediment characteristics, although requirements for site access required the use of a dock at the outside of a meander bend in the Choptank oligohaline zone. Long-term data indicate that salinity ranges from 0 to 5 practical salinity units (psu) 5 km downstream from the oligohaline Choptank River floodplain site and rarely exceeds 0.5 psu on the Pocomoke River at Pocomoke City (9 km up from the downstream oligohaline floodplain site) (http://mddnr.chesapeakebay.net/eyesonthebay/index.cfm).

2.2. Sediment Accretion

[13] Sediment accretion was measured along three to five transects perpendicular to the river channel at each of the four sites on each river. Transects ranged in length from 30 to 50 m with measurement plots located at 10 m intervals along each transect. At each plot, a 2 cm deep, 50 cm × 50 cm marker horizon was created using white feldspar clay powder. The clay becomes a firm, durable marker after it absorbs water and allows accurate measurement of short-term net vertical accretion rates above the clay surface [*Hupp and Bazemore*, 1993]. Marker horizons were installed in April and May 2010 and read in April and May 2011; the period between deployment and measurement was used to calculate the rate of accretion (mm yr^{-1}). The depth of burial of the marker horizons was measured using the cryocore technique [*Cahoon et al.*, 1996] in which a 1 cm diameter copper tube is inserted vertically into the marker horizon, filled with liquid nitrogen, and removed from the ground once a layer of sediment and feldspar has frozen to the outside of the tube. The depth of sediment above the surface of the feldspar was measured to the nearest millimeter. Where sediment deposition was negligible and the feldspar was visible, the cryocore technique was not used. Instead, sediment depth on the marker horizon was measured in situ by slicing through the pad with a knife and exposing a vertical plane for measurement at multiple locations.

2.3. Floodplain Inundation

[14] Water level was measured continuously at each of the eight floodplain sites. A 6.3 cm diameter slotted plastic well casing was installed at a lower elevation location near the middle transect at each site, and a HOBO pressure transducer (accuracy of 5 mm, Onset, Bourne MA) was installed in the well to record measurements at 12 min intervals. Pressure data were converted to water depth by correcting for atmospheric pressure at the Salisbury-Ocean City Wicomico County Regional Airport measured by the National Weather Service Automated Surface Observing System and retrieved from the North Carolina State Climate Office (http://www.nc-climate.ncsu.edu/). The elevation of each sediment accretion sampling plot was surveyed relative to the elevation of the floodplain water level pressure transducer using an optical level. Inundation of each plot during the study period was calculated using three metrics: mean water level during inundation, the percent of time each plot was inundated, and the number of inundation events.

2.4. Hydrology

[15] Channel flow velocity and water level were measured for 1 month on both rivers. Argonaut 500SL (500 kHz) acoustic Doppler current profilers (ADCP) (Sontek/YSI, San Diego, CA) were deployed from docks in the oligohaline zone, and Argonaut 1500SL (1500 kHz) were deployed on pipes driven into the riverbed in the tidal freshwater zone. The Argonaut 500SL has a maximum range of 120 m, and 1500SL has a maximum range of 20 m; both models were programed to measure velocity in 10 horizontal increments

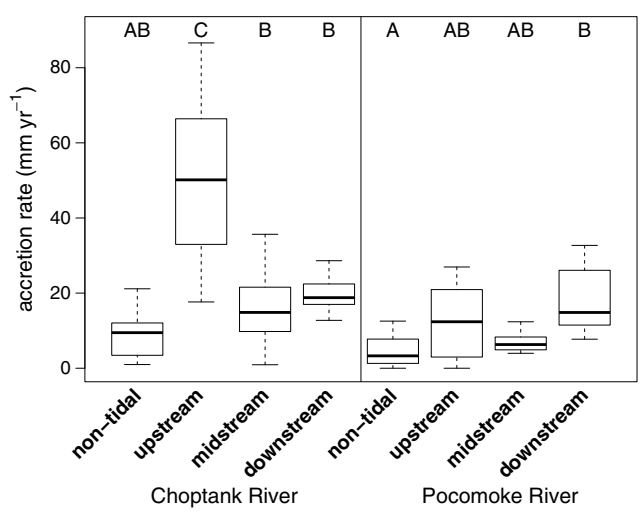

Figure 3. Sediment accretion rates; sites sharing letters indicate those which were not significantly different using a Tukey post hoc test. Solid line indicates the median, box denotes the 25th to 75th quartiles, and bars show the range of samples greater than 1.5 × interquartile range.

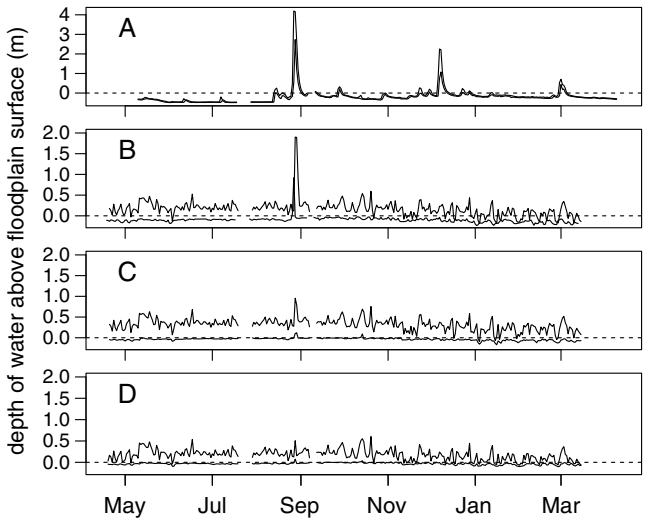

Figure 4. Minimum and maximum daily water level measured on the Choptank River at the (a) nontidal, (b) upstream tidal, (c) midstream tidal, and (d) downstream tidal floodplain sites.

across the channel, with an averaging period of 3 or 4 min. The profiling distance was determined using diagnostic procedures which allow detection of interference from the opposing channel bank. Depth of the Argonaut at the oligohaline zone on the Choptank ranged from 0.4 to 1.6 m below the water surface, while mean water depth was 4 m at the location of deployment. The Argonaut at the oligohaline zone on the Pocomoke ranged from 0.9 to 1.8 m in depth, and mean water depth at the deployment location was 1.8 m. Argonauts were deployed for a 24 h test period following diagnostic setup. Data from this test deployment were examined, deployment configuration was modified as necessary, and then deployment was restarted for a 1 month period. A YSI 600 OMS (YSI Incorporated, Yellow Springs, OH) was deployed with the ADCPs to measure salinity and was calibrated prior to deployment with 1000 Ms cm^{-1} solution. Salinity was used to correct velocity data for the speed of sound.

[16] Argonauts were deployed from 13 September 2011 to 12 October 2011 on the Choptank River; however, the Argonaut malfunctioned at the tidal freshwater zone site during this period and the instruments were redeployed at both Choptank sites from 1 November 2011 to 30 November 2011. Measurements were made from 16 September to 13 October 2011 on the Pocomoke River.

[17] Nontidal river discharge and stage at U.S. Geological Survey (USGS) gaging stations on both rivers was downloaded for the periods of ADCP deployment. Data from the Choptank River (USGS gage number 01491000) was obtained from http://waterdata.usgs.gov/usa/nwis/uv?01491000, and data from the Pocomoke River (USGS gage number 01485000) was obtained from http://waterdata.usgs.gov/usa/nwis/uv?01485000. Suspended sediment concentrations and flow velocity measured at each gage over their period of record were also downloaded from the USGS National Water Information System (nwis.waterdata.usgs.gov/nwis/pmcodes). Monthly SSC measurements at the Choptank River were available from 7 December 1972 to 12 October 2011 and at the Pocomoke River from 23 October 2000 to 29 Apr 2002.

2.5. Riverine SSC and Particle Size

[18] Suspended sediment concentration and particle size were measured over a lunar tidal cycle (24.8 h) at the tidal freshwater and oligohaline sites where channel hydrology was measured. Sampling was conducted between 13 and 16 September 2011 on both rivers, and again on 1 and 2 November 2011 on the Choptank River. Automated samplers (Teledyne Isco, Lincoln, NE) were programmed to collect a 1 L sample every 1 h 2 min over each lunar tidal cycle. At the tidal freshwater zone sites, the intake of the water sampler was attached to the ADCP mounting post and positioned equidistant between the surface and bottom of the water column at low tide; at the oligohaline sites, the Isco tubing intake was >0.5 m below the low tide water level. Water samples were stored on ice, returned to the laboratory, and split using a sample splitter (Geotech Environmental Equipment, Inc, Denver, CO). A 100 ml subsample was used for particle size analysis, and the remainder was used for measuring SSC. Concentration was determined by filtration (American Society for Testing and Materials method D 3977-97) with precombusted 1.5 micron Whatman 934AH filters (47 mm diameter, GE Healthcare Biosciences, Pittsburgh, PA). Samples were dried at 105°C for >12 h. Organic content on the filters was determined by mass loss following combustion at 450°C for 5 h.

[19] A Sequoia Laser In-situ Scattering and Transmissometry (LISST)-100X (Sequoia Scientific, Inc, Bellevue, WA) was used to quantify the volumetric particle size of suspended matter between 1.25 μm and 250 μm within 32 logarithmically distributed size classes. The LISST-100X was deployed for a lunar tidal cycle at the oligohaline zone sites by mounting it to the docks where ADCPs were deployed; depth of deployment averaged 0.4 m at Choptank and 0.9 m at the Pocomoke. Measurements were recorded at 1 min intervals. In the laboratory, subsamples from each of the Isco sampling periods were run on the LISST-100X equipped with a stirring mixing chamber with 60 individual measurements averaged for each sample.

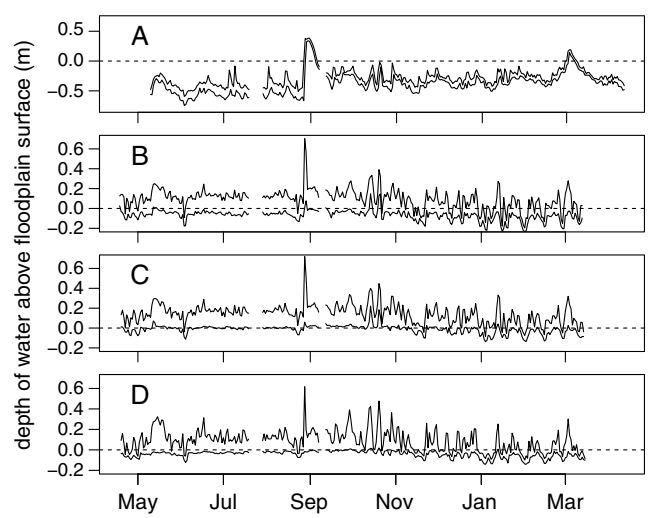

Figure 5. Minimum and maximum daily water level measured on the Pocomoke River at the (a) nontidal, (b) upstream tidal, (c) midstream tidal, and (d) downstream tidal floodplain sites.

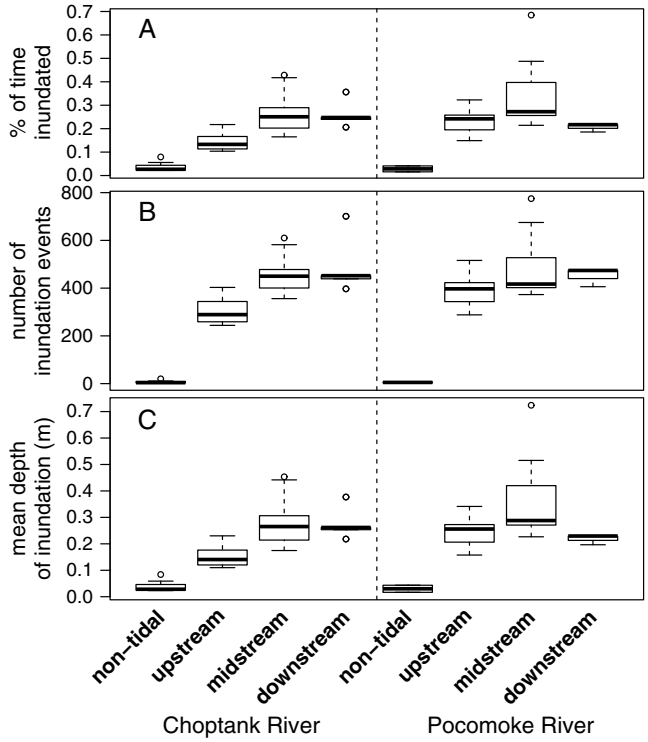

Figure 6. Distribution of (a) percent of measurement period feldspar pads were inundated, (b) the number of times they were inundated, and (c) the mean depth when they were inundated.

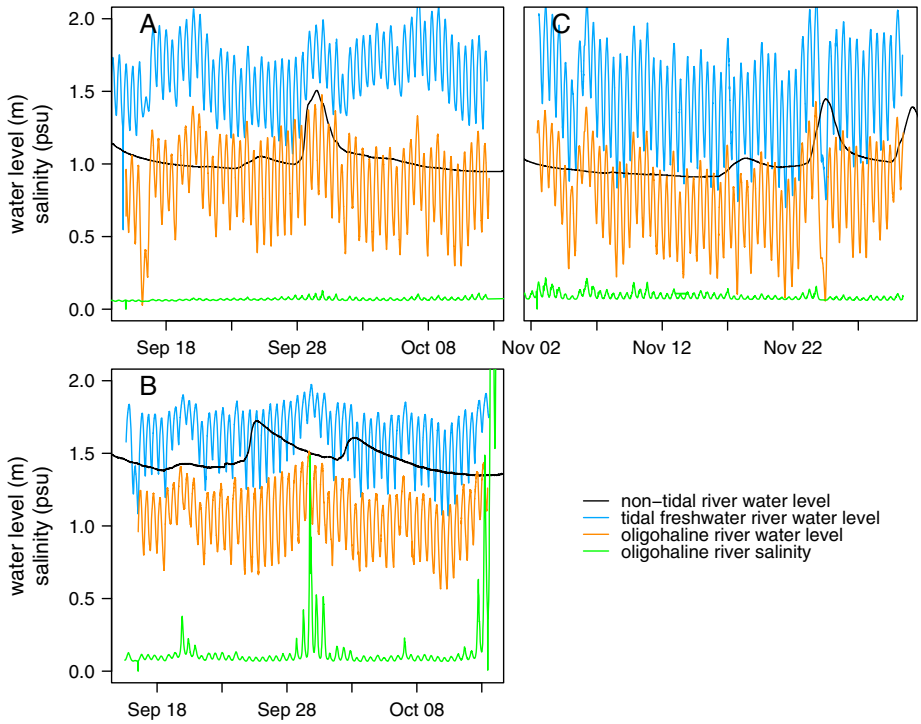

Figure 7. Water level in the channel at the nontidal USGS stream gages and the tidal measurement sites and salinity at the tidal sites on the (a) Choptank River and (b) Pocomoke River in September–October and the (c) Choptank River in November. Water level at the tidal sites is measured relative to an arbitrary datum not comparable across sites or rivers.

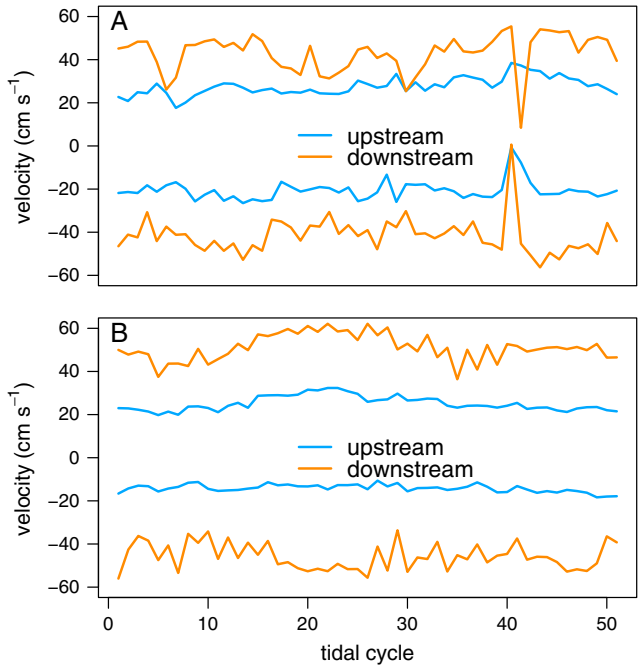

Figure 8. Minimum and maximum current velocity per tidal cycle at the (a) Choptank River sites during October–November and (b) Pocomoke River sites during October–November; positive values indicate ebb flow direction, negative values indicate flood flow direction.

2.6. Backscatter-Derived SSC

[20] ADCP acoustic signal strength was used to calculate the concentration of suspended matter in the channel throughout the 1 month period of ADCP velocity measurements [*Thorne et al.*, 1993; *Reichel and Nachtnebel*, 1994; *Gartner*, 2004]. We used *Urick's* [1975] sonar equation for converting acoustic backscatter signal strength to SSC. In brief, the measured backscatter at the ADCP transducer or reverberation level (RL, raw signal strength in decibels) is corrected for the loss of signal strength from absorption and spreading of the transmitted acoustic signal (transmission loss, TL)

$$\mathrm{TL} = 20\log(R) + 2\alpha R \tag{1}$$

where R is range (m) from the transducer and α is the absorption coefficient (dB m^{-1}). Sound absorption was calculated from observed temperature and salinity using the formula of *Schulkin and Marsh* [1962] excluding pressure as a factor affecting absorption (due to the shallow depth of deployment). The minimum R was greater than the critical range (2 m at 500 kHz and 0.7 m at 1.5 mHz) at which near-field corrections are needed [*Downing et al.*, 1995], and therefore, near-field correction was not calculated. By correcting for transmission losses from the observed backscatter (reverberation level, RL), the relative backscatter (RB) is

$$\mathrm{RB} = \mathrm{RL} + 2\mathrm{TL}. \tag{2}$$

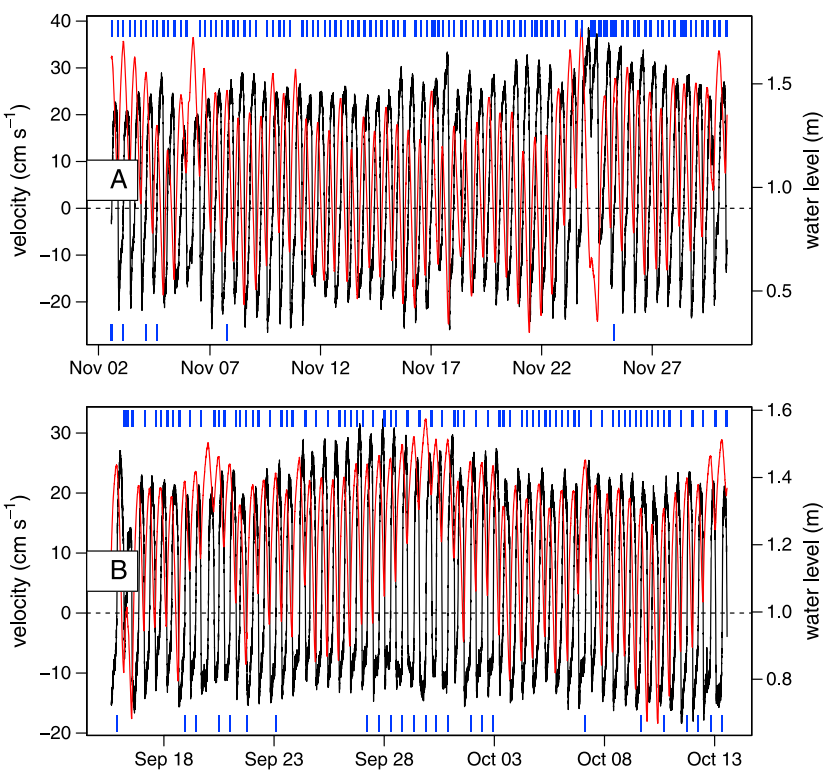

Figure 9. Average current speed and water level at the (a) Choptank tidal freshwater and (b) Pocomoke tidal freshwater sites; red line indicates water level and black line indicates velocity. Blue bars at the top of each panel denote periods with ebb (downstream) current concurrent with rising water level; blue bars at the bottom of each panel denote periods with flood (upstream) current concurrent with falling water level.

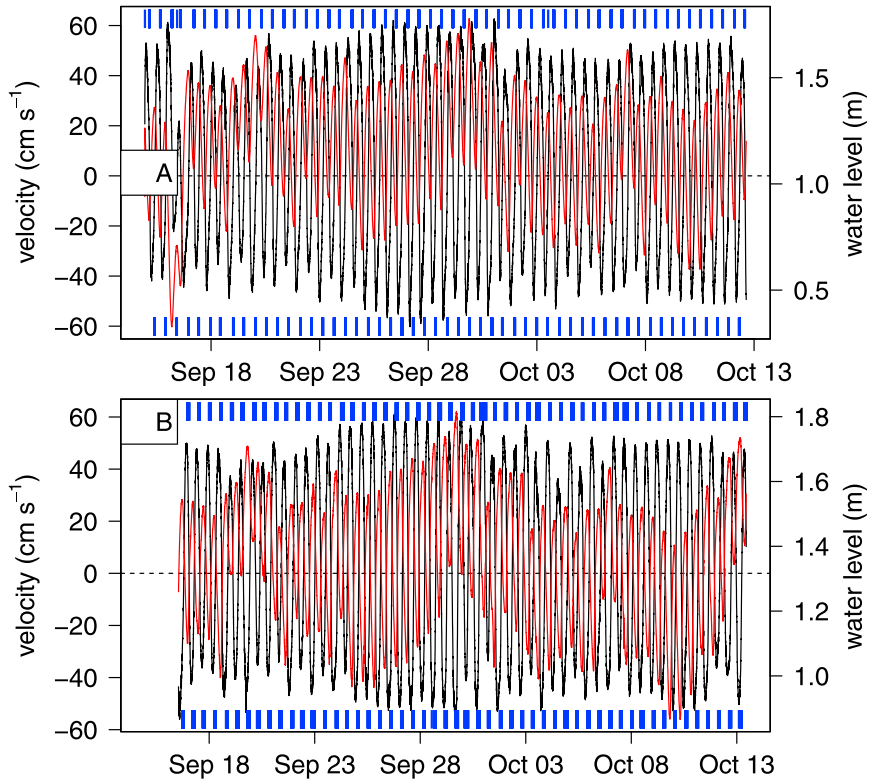

Figure 10. Average current speed and water level at the (a) Choptank oligohaline and (b) Pocomoke oligohaline sites; red line indicates water level and black line indicates velocity. Blue bars at the top of the panel denote periods with ebb (downstream) current concurrent with rising water level; blue bars at the bottom of the panel denote periods with flood (upstream) current concurrent with falling water level.

[21] The relative backscatter strength is a logarithmic function of the particle concentration of the water and can be related using the equation

$$\mathrm{SSC}_{\mathrm{predicted}} = 10^{(A+B\times\mathrm{RB})} \tag{3}$$

where A and B are regression coefficients estimated using least squares regression. The RB from the first profiled cell was used for regression.

[22] In addition to sound absorption by water, RL also is attenuated by suspended sediment [*Urick*, 1975]. This attenuation is a function of particle size, concentration, density, and instrument frequency. Given the maximum observed SSC, mean particle size, and density at the four study sites, and frequency of each site's ADCP maximum attenuation was <0.1%, 12.2%, 3.4%, and 8.9% of RB at the Choptank tidal freshwater zone, Choptank oligohaline zone, Pocomoke tidal freshwater zone, and Pocomoke oligohaline zone, respectively. Like other researchers working in rivers with low suspended sediment [*Wall et al.*, 2008], we elected not to correct for this attenuation of signal strength.

[23] A limitation of deriving SSC from ADCP backscatter data is that the backscatter signal strength is strongly affected by particle size. Particle circumference must be less than the acoustic wavelength (1 mm at 1500 kHz and 3 mm at 500 kHz) for effective acoustic scattering and backscatter signal detection [*Gartner*, 2004]. The sensitivity of the ADCPs to the suspended matter was evaluated by measuring the distribution of particles using the LISST as described above. If measured mean particle sizes were less than these thresholds then we assumed that backscatter signal detection was possible at the study sites.

[24] The across-channel SSC predictions based on backscatter data were averaged for each measurement interval. Application of the observed SSC backscatter regression to backscatter data collected across the width of the channel required the assumption that the size distribution and composition of SSC did not vary laterally across the channel.

2.7. Statistical Analysis

[25] We examined the effect of river ($n=2$), site along the tidal gradient ($n=4$), and distance from the channel ($n=5$) on sediment accretion rate using analysis of variance (ANOVA). Normality was examined using Shapiro's test, and data were normalized by square or cubed root transformation when necessary. Model simplification was performed using sequential F tests ($\alpha=0.05$) and comparing model performance under iterations with different model terms deleted. Differences between measured SSC (total, organic, and inorganic) and mean particle size between the oligohaline zone and tidal freshwater zone on each river were examined using t tests ($\alpha=0.05$) for normally distributed data and a Wilcox test for nonnormally distributed data. A Kruskal-Wallis test was used to examine differences in predicted SSC at different tidal stages followed by the post hoc pairwise comparison test (Tukey test) described in *Siegel and Castellan* [1988]

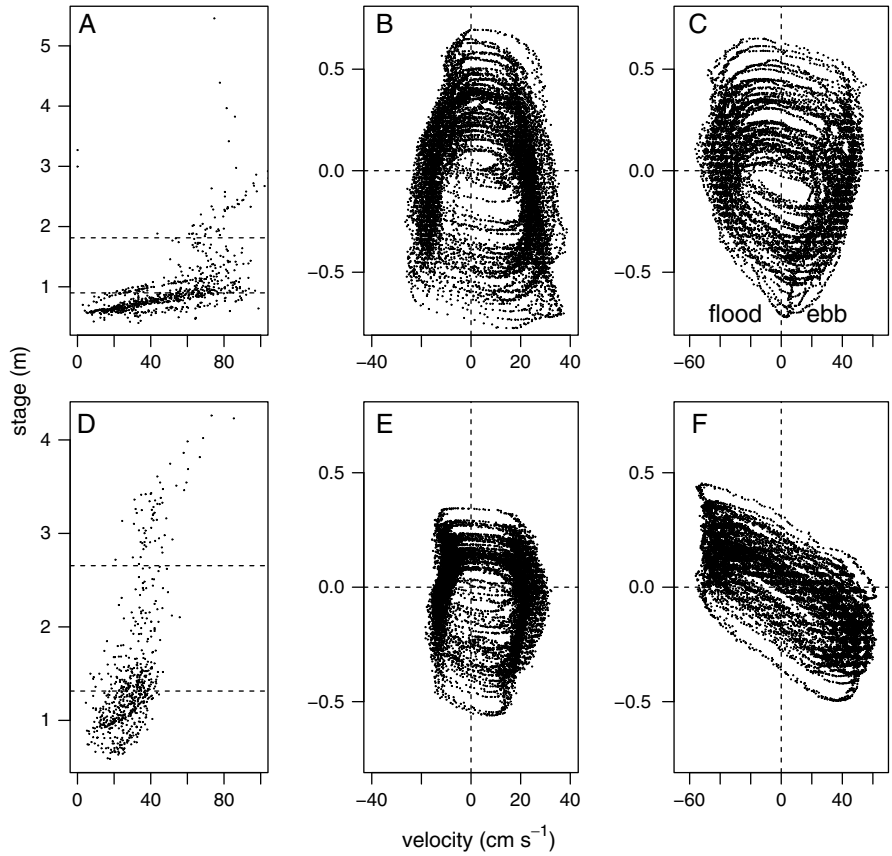

Figure 11. Flow velocity versus stage at the (a) nontidal Choptank River at Greensboro USGS gage, (b) upstream tidal Choptank River, (c) downstream tidal Choptank River, (d) nontidal Pocomoke River at Willards USGS gage, (e) upstream tidal Pocomoke River, and (f) downstream tidal Pocomoke River. Data shown in Figures 2a and 2d are for all observations made at these gaging stations since their inception, and horizontal lines bracket the river stage that was reported during our tidal measurements.

and implemented in a statistical package for R (*Giraudoux*, unpublished data, 2013, http://cran.r-project.org/web/packages/pgirmess/index.html). All statistical and graphical analyses were performed using R [*R Development Core Team*, 2009].

3. Results

3.1. Sediment Accretion Rates

[26] Distance from the channel along the transects was not a significant term in the model explaining accretion rates, and therefore, the final statistical model included only river and site with an interaction term (Table 1). Riparian accretion rates were significantly greater on the Choptank (24 ± 20 mm yr^{-1}, mean and standard deviation) than the Pocomoke River (13 ± 16 mm yr^{-1}). Riparian accretion rates also differed among river sites. Mean and standard deviation of the nontidal, upstream, midstream, and downstream sites (combining both rivers) was 8 ± 8 mm yr^{-1}, 33 ± 28 mm yr^{-1}, 12 ± 9 mm yr^{-1}, and 19 ± 8 mm yr^{-1} (Figure 3). A post hoc test indicated that the upstream site on the Choptank was significantly greater than all other sites, while the nontidal Pocomoke was significantly less than the downstream Pocomoke and all tidal Choptank sites (Figure 3).

3.2. Floodplain Inundation

[27] In late August 2011, heavy rainfall associated with Hurricane Lee passed over the region and resulted in a ~4 m deep flood at the nontidal floodplain of the Choptank River (Figure 4a), but only a ~0.4 m deep flood on the nontidal Pocomoke floodplain (Figure 5a). The maximum flooding depth during this event decreased throughout the tidal portion of the Choptank River but was never apparent at the downstream site (Figure 4d). While the depth of flooding was more moderate at the tidal Pocomoke River sites (~0.6 m), the depth of flooding did not diminish along the tidal gradient although the flood was only evident for 1 tidal cycle (Figure 5d). The daily range in inundation depth was greater during May through November period than the rest of the year.

[28] The percent of time the floodplain sites were inundated, the number of inundation events, and the mean flooding depth increased from the nontidal site to the downstream site at plots on the Choptank River (Figure 6). Along the Pocomoke River, these three metrics of inundation were greatest at the upstream and midstream tidal sites. Inundation metrics could only be calculated for plots that were higher in elevation than the location of the pressure transducer, and therefore, the metrics do not include all of the plots at each site. Therefore, the median

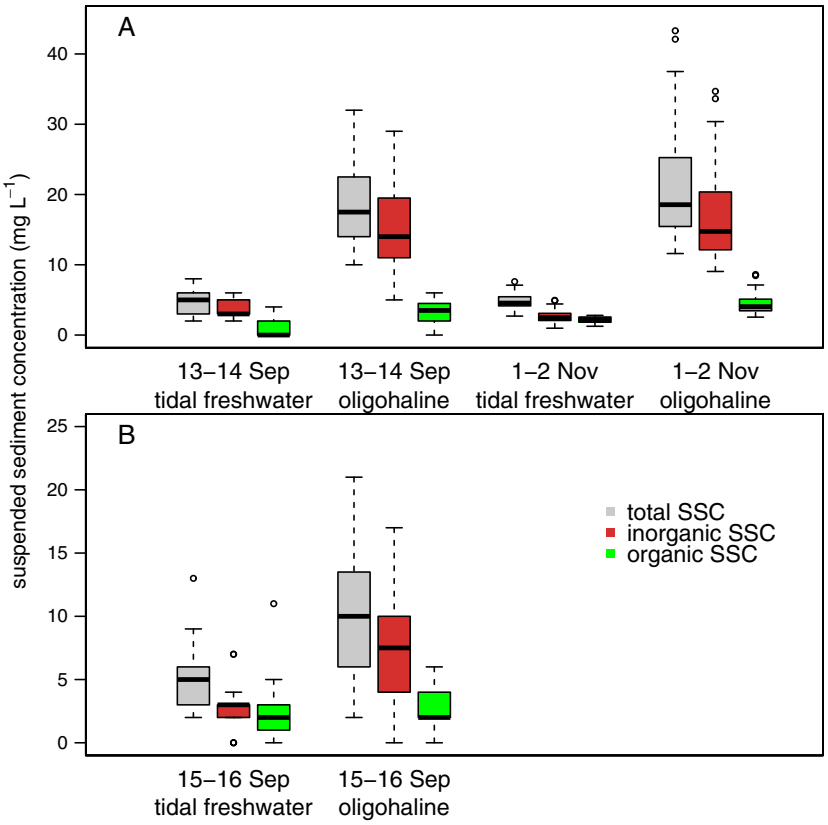

Figure 12. Total, organic, and inorganic suspended sediment concentration measured in automatically collected water samples over a 24.8 h period on the (a) Choptank River and (b) Pocomoke River.

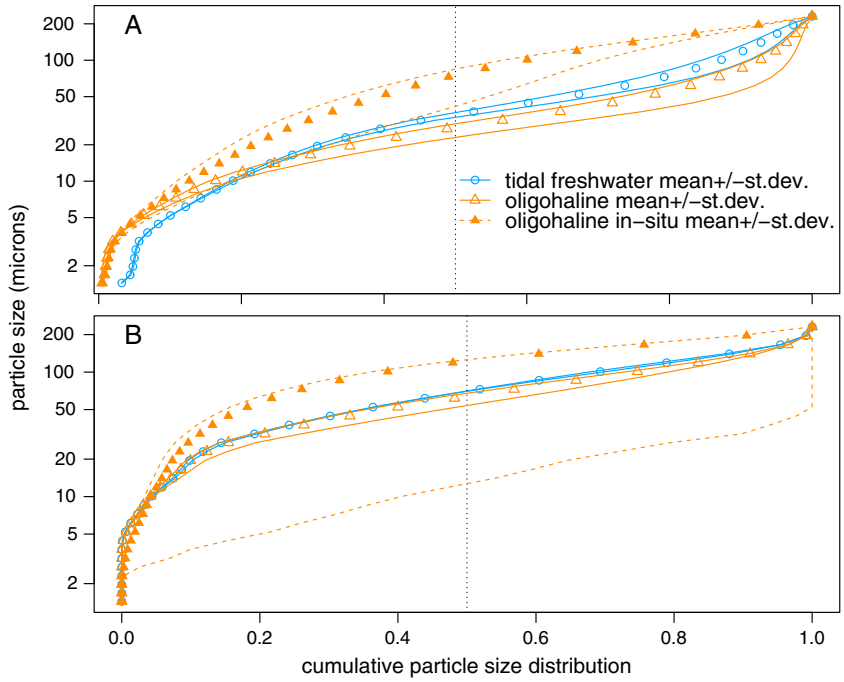

Figure 13. Cumulative distribution of particle size measured during in situ deployment of LISST and laboratory measurement made on automatically collected water samples over a 24.8 h period on the (a) Choptank and (b) Pocomoke Rivers. Points represent means, and lines indicated 1 standard deviation of the mean.

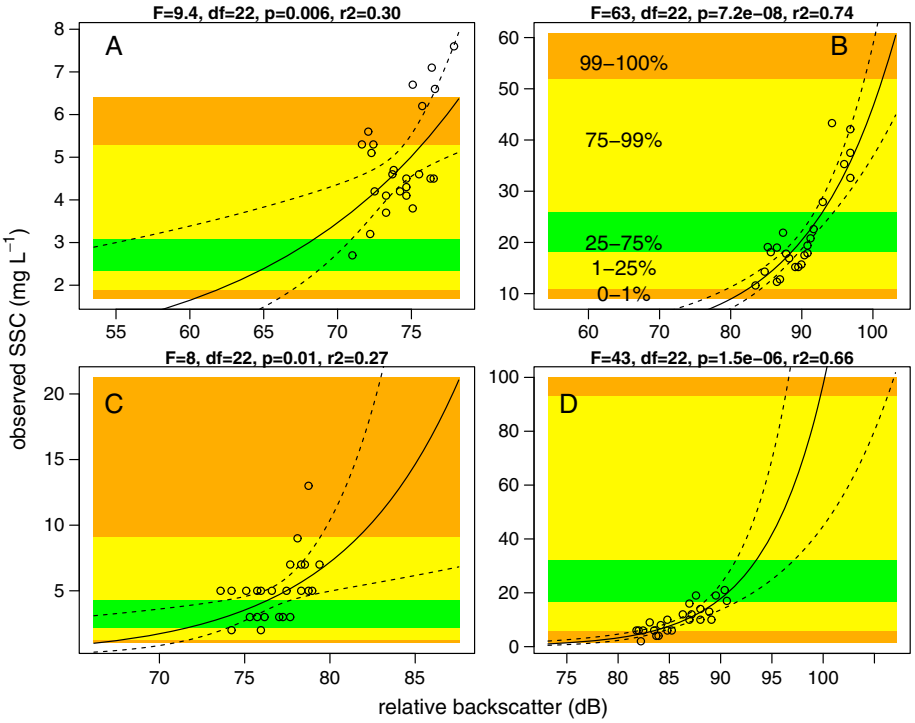

Figure 14. Observed SSC versus relative backscatter from ADCP at the (a) tidal freshwater Choptank, (b) oligohaline Choptank, (c) tidal freshwater Pocomoke, and (d) oligohaline Pocomoke. Solid lines show the predicted SSC (equation (3)) across the range of relative backscatter observed over the month of observation; dashed lines show the 95% confidence interval. Color bands denote the quantiles (labels in Figure 14b) of all predicted SSC values during the 1 month period (except at the oligohaline Pocomoke where the *y* axis has been abbreviated from 200 to 100 mg L^{-1}). Statistics at the top of each panel show results of the regression between observed SSC and relative backscatter.

and ranges are underestimates of all three metrics, because plots not included in this analysis were inundated more frequently and to a greater depth because of their lower elevation.

3.3. Channel Hydrology

[29] Storm events occurred in both the Choptank and Pocomoke Rivers during the September–October and November measurement periods (Figure 7). These peaks in water level in the nontidal river corresponded with increased water level in the tidal Choptank River, but not in the Pocomoke River. The tidal amplitude fluctuated throughout the study on both rivers with higher amplitude on the Choptank than Pocomoke River. Mean salinity at the tidal freshwater Choptank and Pocomoke Rivers was 0.05 psu and 0.06 psu, with maximum of 0.06 psu at both sites. Throughout both periods of study, mean and maximum salinity at the oligohaline Choptank River were 0.08 psu and 0.22 psu, respectively. At the oligohaline Pocomoke River, mean and maximum salinity were 0.21 psu and 4.4 psu, respectively.

[30] Average maximum flow velocities during ebb and flood on the tidal freshwater Choptank River were 27.7 cm s^{-1} and 20.7 cm s^{-1}, respectively, and 43.0 cm s^{-1} and 41.7 cm s^{-1} on the oligohaline Choptank River during October and November (Figure 8). At the tidal freshwater Pocomoke River, maximum flow velocity was 25.1 cm s^{-1} during ebb tide and 14.2 cm s^{-1} during flood tide; corresponding values at the oligohaline Pocomoke were 51.1 cm s^{-1} and 45.8 cm s^{-1}, respectively. The tidal freshwater zones on both rivers were always ebb dominant (fastest flow velocity during ebb tide), but the oligohaline zones exhibited flood dominance (fastest flow velocity during flood tide) during 5 of 53 tides on the Choptank in September–October, 14 of 54 tides on the Choptank in November, and during 8 of 52 tides on the Pocomoke River.

[31] Ebb flow lagged behind falling stage on a few occasions on the tidal freshwater Choptank River, but flood flow lagged behind rising stage regularly, averaging 37 min per tidal cycle (Figure 9a). Tidal dynamics in the tidal freshwater Pocomoke were similar, except that flood flow lagged rising stage by an average of 25 min per tidal cycle (Figure 9b). On the oligohaline Choptank, ebb flow lagged falling stage by an average of 39 min per tidal cycle, while flood flow lagged rising stage by an average of 24 min (Figure 10a). Lag times in the oligohaline Pocomoke were more than double than those on the oligohaline Chopank: Ebb flow lagged falling stage by 103 min per tidal cycle, and flood flow lagged rising stage by 103 min per tidal cycle on the oligohaline Pocomoke River (Figure 10b).

[32] The hysteresis between tide stage and current velocity demonstrated that maximum flow velocity in the Choptank River tidal freshwater and oligohaline zones occurred around midtide (Figures 11b and 11c). A similar pattern occurred in the tidal freshwater Pocomoke River, but within its oligohaline zone, the Pocomoke River exhibited peak flow velocity during high tide and low tide (Figures 11e and 11f). Stage-velocity

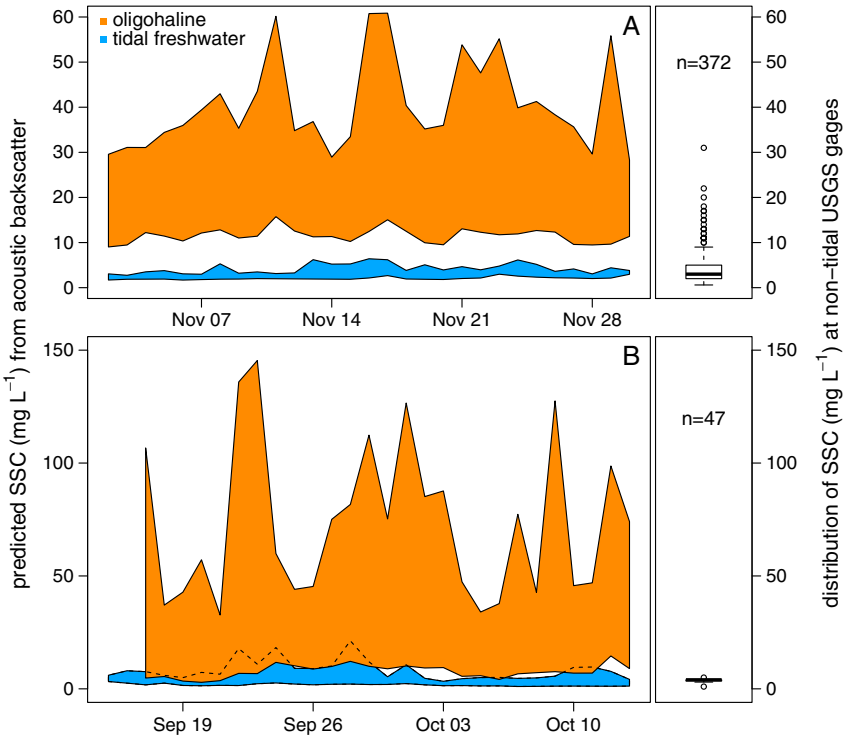

Figure 15. Range in daily SSC at the (a) Choptank sites and (b) Pocomoke sites; a 15 min moving average was applied to the Pocomoke oligohaline site to average out extreme values. Side bars show the distribution of SSC at the USGS nontidal stream gages during their period of record for discharge equal or less than that observed during the current study.

relationships at the nontidal gaging stations show varying degrees of a positive relationship between stage and velocity (Figures 11a and 11d).

3.4. Measured SSC

[33] Over a lunar cycle in September, the tidal freshwater Choptank and Pocomoke Rivers had similar total SSC (Wilcox $W=278$, $p=0.84$) but the Choptank had higher inorganic SSC ($W=406$, $p=0.01$) while the Pocomoke had higher organic SSC ($W=153$, $p=0.004$) (Figure 12). The oligohaline Choptank River had higher total and inorganic SSC than the oligohaline Pocomoke ($W=480$, $p=7.4\times10^{-5}$ and $W=491$, $p=3.0\times10^{-5}$, respectively), but there was no difference in the organic SSC ($W=331$, $p=0.37$). In water samples from the Choptank River in September, total ($W=0$, $p=2.6\times10^{-9}$), inorganic ($W=7.5$, $p=6.1\times10^{-9}$), and organic SSC ($W=101$, $p=6.5\times10^{-5}$) were significantly greater in the oligohaline versus tidal freshwater zone, and the same pattern was found in November ($W=0$, $p=3.0\times10^{-9}$, $W=0$, $p=6.2\times10^{-14}$, and $W=12$, $p=1.3\times10^{-8}$, respectively). Water samples from the Pocomoke River in September also had higher total ($W=101$, $p=0.0001$) and inorganic SSC ($W=84$, $p=2.1\times10^{-5}$) in the oligohaline versus tidal freshwater zone, although there was no significant difference between sites in organic SSC ($W=220$, $p=0.14$).

[34] Particle size of suspended matter in automatically collected water samples in the Choptank River in November was significantly greater ($t=7.1$, df$=44$, $p<0.0001$) in the tidal freshwater zone (mean diameter$=53$ µm) than oligohaline zone (mean diameter$=41$ µm) (Figure 13). Mean particle size in the Pocomoke River was also larger in the tidal freshwater zone (mean$=84$ µm) than oligohaline zone (mean$=76$ µm, t$=4.5$, df$=44$, p<0.0001). These results were obtained from automatically collected samples which may have differed from in situ particle size. To investigate the effects of collection and storage on particle size, we compared the mean particle size of samples collected from the oligohaline Choptank River (41 µm) with in situ measurements made at the time of sample collection (68 µm; a similar comparison could not be performed for the Pocomoke River). Regression analysis showed a significant relationship ($F=42$, df$=22$, $p=1.5\times10^{-6}$, $R^2=0.66$) between these data, with an intercept of 10.4 (±standard error of 4.7) and slope of 0.34 (±0.05). Therefore, our analysis of stored water samples underestimated mean particle size from that found in situ by 66% on average in the lower Choptank River.

[35] Measured mean particle size was used to evaluate the effectiveness of the acoustic backscatter method of predicting SSC. Mean particle size was less than the acoustic wavelength at all sites, even when particle size was assumed to be 66% greater to account for interference from sampling and storage of water prior to analysis. Therefore, the majority of the suspended sediment in suspension provided optimal conditions for reflectance of the acoustic signal back to the ADCP, and an important requirement for using acoustic backscatter to predicted SSC was met.

3.5. Predicted SSC

[36] Suspended sediment concentration over monthly deployments of ADCPs was predicted from the relationship between observed SSC and signal backscatter calculated using equation (3) for each site. All regression relationships

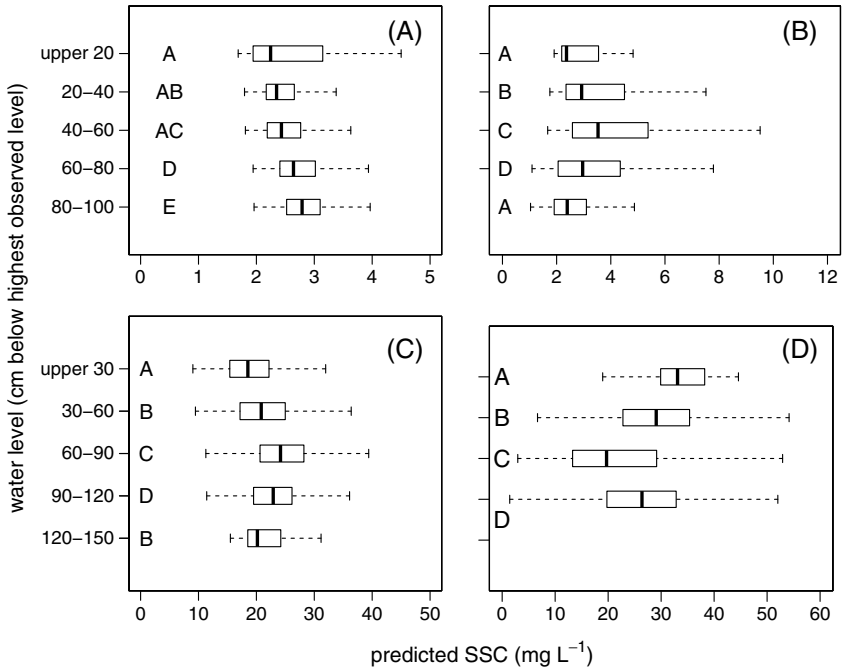

Figure 16. Distribution of predicted SSC at different water levels on the (a) Choptank River tidal freshwater in September–October 2011, (b) Pocomoke River ridal freshwater during November 2011, (c) Choptank River oligohaline in September–October 2011, and (d) Pocomoke River oligohaline during November 2011. Increments sharing the same letter denote groups that were not statistically different based on a nonparametric post hoc test.

were significant, however R^2 values were 0.30 and 0.27 at the tidal freshwater Choptank and Pocomoke sites, respectively, and 0.74 and 0.66 at the oligohaline Choptank and Pocomoke sites, respectively (Figure 14). At the tidal freshwater sites on both rivers, the majority of the predicted SSC values over the 1 month period were less than the observed SSC during the 24.8 h calibration period due to temporal variation in SSC (Figures 14a and 14c). At the tidal freshwater Choptank site, the 95% confidence interval (CI) of the median SSC prediction (3.1 mg L^{-1}) was 2.3–4.2 mg L^{-1}. On the tidal freshwater Pocomoke, the 95% CI of the median-predicted SSC (1.8 mg L^{-1}) was 0.9–3.6 mg L^{-1}. The oligohaline Choptank SSC calibration data set encompassed nearly 98% of the range in SSC predicted during the month of monitoring, and therefore, the corresponding SSC prediction errors were relatively small for the majority of the samples collected (Figure 14b). For example, the median-predicted SSC (21 mg L^{-1}) had a 95% CI of 22–26 mg L^{-1}. Of the four sites studied, prediction error was largest at the oligohaline Pocomoke, where the SSC calibration data set spanned only the lower 25% of the predicted SSC values (Figure 14d). Prediction error of the median-predicted SSC at the oligohaline Pocomoke (31 mg L^{-1}) was 20–47 mg L^{-1}, while the 75th percentile of predictions (41 mg L^{-1}) had a 95% CI of 24–67 mg L^{-1}.

[37] Predicted SSC over the 1 month deployments was always greater at the oligohaline site on each river than simultaneous predictions at the tidal freshwater site (Figure 15). SSC at the tidal freshwater sites was within the range of values reported at the nontidal USGS gaging stations. The oligohaline sites exhibited SSC that was generally greater than the 75th percentile of measurements made at the USGS gaging station. Only extreme values of SSC from the nontidal gage on the Choptank River exceeded the minimum daily SSC in the oligohaline Choptank River.

[38] Predicted SSC varied with water level differently on the Choptank and Pocomoke Rivers. We separated the predicted SSC measurements into four or five increments of tidal stage, with the upper increment reflecting the stage at which the floodplain was inundated. On the tidal freshwater Choptank and Pocomoke Rivers, this first increment was the upper 20 cm of water level (based on measurements at the upstream and midstream floodplain sites, Figure 6), and at the oligohaline zone, it was the upper 30 cm (based on measurements at the downstream floodplain site). In the tidal freshwater, Choptank River predicted SSC was highest when tide stage was at the lowest 40 cm of the tidal range (Kruskal-Wallis chi-squared = 1237, $p < 2.2 \times 10^{-16}$, Figure 16a). In the oligohaline Choptank River, predicted SSC was significantly lower when the floodplain was inundated than during the rest of the tidal cycle (Kruskal-Wallis chi-squared = 756, $p < 2.2 \times 10^{-16}$, Figure 16b). The tidal freshwater Pocomoke River followed a similar trend: Lowest predicted SSC occurred at the highest and lowest water level (Kruskal-Wallis chi-squared = 629, $p < 2.2 \times 10^{-16}$, Figure 16c). In contrast, the oligohaline Pocomoke River exhibited the opposite trend: Highest predicted SSC occurred when the floodplain was inundated (Kruskal-Wallis chi-squared = 1359, $p < 2.2 \times 10^{-16}$, Figure 16d). Furthermore, there was significantly higher predicted SSC at the oligohaline Pocomoke River (median = 30 mg L^{-1}, mean = 28 mg L^{-1}) than the oligohaline Choptank River (median = 18 mg L^{-1}, mean = 18 mg L^{-1}) during floodplain inundation (Wilcox test excluding values over 41 mg L^{-1} SSC, the 75th percentile, on the Pocomoke River; w = 413093, $p < 2.2 \times 10^{-16}$).

4. Discussion

4.1. Sediment Transport and Accretion in Weakly and Strongly Convergent Tidal Rivers

[39] We expected to find differences in tidal dynamics, sediment transport, and resultant sediment accretion between tidal rivers with standing and progressive waves [*Savenije*, 2005; *Hughes*, 2012]. With a lag period of only 39 min between the beginning of ebb flow and falling stage, the oligohaline Choptank River is close to exhibiting a standing wave, whereas the oligohaline Pocomoke River's 103 min lag reflects a more progressive wave. As expected, these wave characteristics corresponded with tidal river morphology, where the strongly convergent Choptank River demonstrated a standing wave, and the weakly convergent Pocomoke River exhibited the more progressive wave.

[40] The contrast in tidal dynamics between the Choptank and Pocomoke was also apparent in the trend in SSC over the tidal range, particularly at the oligohaline sites. Assuming that SSC is a function of flow velocity, we expected that SSC would be highest during periods of the tidal cycle when flow velocity was highest. The highest SSC in the oligohaline Choptank occurred during midtide when flow velocity was fastest. In contrast, highest SSC in the oligohaline Pocomoke River occurred during high and low tide when flow velocity was fastest. The more progressive wave in the Pocomoke River corresponded with higher SSC than the Choptank River during the tide stage at which riparian wetlands were inundated.

[41] We expected that the river with higher SSC during tidal inundation of wetlands would also have higher sediment accretion rates. We found the opposite: The Choptank River with lower SSC during wetland inundation had higher sediment accretion than the Pocomoke River. This result was likely influenced by the larger impact of Hurricane Lee on discharge and resultant sediment flux in the Choptank River than the Pocomoke River, and obscured our ability to compare the influence of tidal wave characteristics. The high sediment accretion rates that occurred at the upstream Choptank site, despite the remarkably low measured and predicted SSC at this site, suggest that the single runoff event following Lee may have been responsible. It remains unknown how high-frequency, low-magnitude tidal flooding events compare with low-frequency, high-magnitude river discharge events in the long-term distribution of suspended sediment to tidal wetlands in these rivers. While we did not find evidence of higher sediment accretion associated with progressive wave characteristics, we believe that the mechanistic link between tidal dynamics, SSC, and floodplain sediment accretion remains a reasonable hypothesis for further study in a larger sampling of tidal rivers. The possibility of making broad-scale, general predictions of the sensitivity of estuarine and fluvial habitats to sea level rise based on easily obtainable morphologic and hydrologic data is an alluring possibility that warrants further investigation.

[42] Our efforts to integrate tidal hydrology with fluvial and wetland morphology in this study emphasized the river-ine-wetland system at the scale of a river reach (nontidal through oligohaline estuary). Our interpretation of the stage-velocity data, their relationship to sediment transport and wetland accretion, and tidal wave characteristics are based on phenomenon described by a broad literature on estuarine morphodynamics (reviewed by *Hughes* [2012]). While the hydrogeomorphic evolution of tidal freshwater wetlands has been reviewed by *Pasternack* [2009] [see also *Pizzuto and Rogers*, 1992; *John and Pizzuto*, 1995], there has been little attention to the fluvial, tidal, and wetland processes at a scale that integrates morphodynamic feedback between freshwater river and wetland morphology with tidal hydrology. Conceptual models of estuarine evolution have been extending into the fluvial-estuarine transition zone [e.g., *Dalrymple and Choi*, 2007], but there is little empirical data describing geomorphic patterns across this transition. Mathematical models [e.g., *Lanzoni and Seminara*, 2002] and physical models [e.g., *Tambroni et al.*, 2005] of tidal channel evolution that incorporate morphodynamic feedback may help inform our understanding of tidal freshwater rivers. However, previous studies have not considered this evolution from the initial condition of a nontidal, fluvial system where river floods overlap with tidal dynamics. In summary, we suggest that future research on tidal freshwater rivers and wetlands focus on hydrogeomorphic feedback in the fashion that estuarine geomorphology has focused on how tides shape estuaries and how estuaries shape tides.

4.2. Spatial Gradients in Floodplain Sediment Accretion and SSC

[43] A second focus of this study was to examine the spatial gradients in floodplain sediment accretion and SSC from the nontidal river through oligohaline estuary. We found two peaks in sediment accretion: the first at the upstream portion of the tidal freshwater zone and the second at the oligohaline estuary downstream. We found two minima in sediment accretion: the nontidal river and the TFFW mid-stream along the tidal gradient. Higher accretion at the oligohaline marshes were expected based on its proximity to the ETM and the high density of macrophyte stems [*Darke and Megonigal*, 2003; *Gellis et al.*, 2008; *Ensign et al.*, 2013b]. The relatively low rates midstream were also not unexpected based on research in other rivers which compared TFFW with upstream nontidal wetlands in the Pocomoke River [*Kroes et al.*, 2007] and a broader survey of TFFW in the Southeastern U.S. [*Craft*, 2012; *Ensign et al.*, 2013b].

[44] The patterns in accretion rate, combined with measurements of in-channel hydrology, allow us to infer two different mechanisms responsible for the two peaks in sediment accretion. At the nontidal to tidal transition, storm events loaded sediment into the tidal river and prolonged residence time and repeated inundation of the riparian zone allowed for increased deposition on the floodplain. The repeated inundation of the site is evident from the time series of water level on both rivers following the rainfall associated with Hurricane Lee, where normal tidal flooding of the tidal sites resumed within 1–2 days even while the nontidal river sites were continually flooded. While we did not measure flow velocity in the tidal river during this event, the resumption of normal tidal inundation indicates that flow velocities were suppressed during the change of tide stage. This lower flow velocity would have allowed deposition of the watershed-derived suspended sediment load. Sediment concentrations in the tidal river channel were low in the tidal freshwater Choptank and Pocomoke during base flow and moderate storm runoff events, indicating that sediment accretion at the upstream tidal sites occurred predominantly during

Hurricane Lee. In contrast, the nontidal site, which is positioned within a narrower valley than the tidal sites, likely experienced higher water velocities on the floodplain during storm inundation that limited deposition.

[45] A second mechanism operated in the tidal river downstream that enhanced sediment accretion in the oligohaline marshes. The higher flow velocities found near the oligohaline marshes were presumably able to erode more material from the bed and banks of the channel and keep this material in suspension. This higher velocity, combined with flocculation of suspended sediment [*Eisma*, 1986], which was suggested by the coarser particle sizes measured in situ than in water samples returned to the lab, generated high SSC composed of large particles during overbank flow into the marsh and greater sediment accretion relative to the TFFW. The high stem density in marshes contributes to high hydraulic roughness which causes deposition of particulates [*Leonard*, 1997; *Leonard and Reed*, 2002]. The high SSC in this portion of the rivers is indicative of the tide-dominated turbidity maximum zone, which can temporarily generate net upstream sediment transport occurs [*Guézennec et al*., 1999; *Geyer et al*., 2001; *Chen et al*., 2005]. In addition to these tidal processes, *Yarbro et al*. [1983] determined by mass balance modeling that much of the suspended sediment in the Choptank River in the vicinity of our oligohaline site was produced by bank erosion within the oligohaline reach of the estuary. They also found that fluvially transported watershed sediment was a minor component of the sediment budget of the Choptank, a conclusion similar to the one we reached by comparison of SSC in the oligohaline versus tidal freshwater river. In the Pocomoke River, research has suggested that TFFW accretion is supported in part by material from downstream [*Kroes et al*., 2007; *Gellis et al*., 2008]. In summary, sediment accretion in oligohaline marshes is a result of high SSC in the channel generated by tidal hydrodynamics and does not appear to be a direct result of watershed sediment export.

[46] Between the zones of high sediment accretion in the upstream and downstream portions of the tidal river, the midstream portion showed the lowest rates of sediment accretion. This region of river and its fringing TFFW may be deprived from the watershed-derived sediment loads due to trapping of sediment in the tidal river upstream, yet may be too far upstream to receive sediment subsidy by the hydraulics within the oligohaline zone. The low rates of sediment accretion in these TFFWs were similar to those found in other studies [*Craft*, 2012; *Ensign et al*., 2013b]. The implications of these low accretion rates for the response of coastal rivers to sea level rise is discussed next.

4.3. Effects of Sea Level Rise on TFFWs

[47] Spatial patterns in sediment accretion across the nontidal river to oligohaline estuary gradient provide insight into the potential geomorphic changes induced by sea level rise in tidal rivers. While sediment accretion does not necessarily equate to a change in wetland surface elevation due to shallow and deep subsidence, we found that the middle portion of the tidal freshwater gradient we studied was most susceptible to submergence as sea level rises due to relatively low rates of sediment accretion. Previous studies have also found rates of short- and long-term sediment accretion in TFFW that are less than the rate of sea level rise [*Baldwin*, 2009; *Craft*, 2012]. The important finding of our study was that accretion rates near the nontidal/tidal boundary are higher than in TFFW farther downstream presumably due to the slower velocities and repeated floodplain inundation which enhances deposition of storm event-derived watershed sediment. Accretion rates are not homogeneous along the length of tidal rivers or even between similar habitats (such as TFFW) located at different ends of the tidal river, and efforts to model the effects of sea level rise will need to account for these gradients in accretion and resultant elevation change.

[48] How will TFFW be affected by the predicted doubling in the rate of sea level rise over the next 100 years [*Vermeer and Rahmstorf*, 2009]? From an ecological standpoint, it is the spatial extent of TFFW which is of primary concern, involving both the loss of existing TFFW and the creation of new TFFW as tides extend into previously nontidal river. Loss of existing TFFW may occur in two ways: the erosion of river shoreline and lateral wetland retreat (i.e., inundation, sensu *Flick et al*. [2012]) and the replacement of TFFW with freshwater and oligohaline marsh [*Krauss et al*., 2009; *Cormier et al*., 2012]. Inundation may be due to lateral erosion and meandering of the river channel and an increase in water depth that prevents aquatic plant growth. Channel bank erosion and meander migration rate have not been well characterized in tidal freshwater rivers, but one study reported a rate of $0.32\,\mathrm{m\,yr^{-1}}$ for tidal freshwater marsh channels [*Garofalo*, 1980]. Yet as sea level extends upstream into previously nontidal channels, stream power may be suppressed by tidal flows and limit channel erosion [*Phillips and Slattery*, 2006; *Ensign et al*., 2013a]. Over time as channels adjust to tidal flows, tidal wave characteristics, such as the relationship between stage and current velocity, may have different effects on bank erosion in tidal channels due to different timing of peak flow during tidal inundation [*Ahnert*, 1960; *Chen et al*., 2011]. Ultimately, these processes lead to the loss of TFFW and increase in channel volume. For example, inundation (conversion to open water) is accounted for the loss of 24% of the tidal wetlands (saltwater and freshwater) in North Carolina between 1994 and 2001 [*Carle*, 2011].

[49] In spite of these mechanisms of tidal wetland loss, TFFWs may be created as tides extend farther inland [*Williams et al*., 1999; *Craft et al*., 2009]. The sediment accretion rates we measured in these nontidal forests, and those by previous research in coastal plain rivers [*Noe and Hupp*, 2005, 2009], are in many cases less than the rate of sea level rise. Thus, even the contemporary rate of sea level rise is adequate to begin flooding the riparian forests at the head-of-tide whose elevation is equal to sea level. However, the subsequent tidally induced changes in hydrology and sediment transport once flooding begins may alter the accretion rate (as we observed in the upper tidal zone) and affect further tidal flooding. The sequence of geomorphic changes that occurs during this transformation is unclear, and the subject remains a particularly important topic for determining how accelerated sea level rise will affect the net distribution of TFFW.

[50] The changes in wetland and channel morphology over time as tides advance farther upstream may reinforce the tidal regime (i.e., progressive wave, standing wave) through geomorphic feedback. For example, a river with a progressive tidal wave that facilitates over-bank delivery of suspended sediment may maintain a sinuous, meandering channel over time even as sea level rises. This deep, sinuous channel

may help maintain an overall channel length longer than 1 quarter the tidal wavelength, and the progressive wave characteristics may persist via this positive feedback. Alternatively, if inundation of the riparian zone and an associated increase in intertidal area and channel volume occurs, then sinuosity and mean channel depth may decrease. These morphologic changes may decrease the channel length, increase convergence and friction, and alter the progressive tidal characteristics to a standing wave tidal regime.

4.4. Conclusions

[51] This study presents four conclusions regarding the spatial patterns in sediment accretion, hydrology, and suspended sediment transport through the tidal freshwater zone. First, TFFW in the lower reaches of tidal rivers have relatively low rates of sediment accretion and are at more risk to sea level rise than oligohaline marshes. However, sediment accretion in the upper TFFW near the head of tide is higher than TFFW downstream due to episodic delivery of sediment from the watershed and forced deposition by the tidal flow regime. Second, sediment accretion rates in TFFW downstream are low because their watershed sediment supply is trapped by TFFW upstream near the head of tide, and they are upstream of the ETM which supplies the oligohaline marshes with sediment. Third, a strongly convergent tidal river with standing wave characteristics exhibited peak flow velocity around midtide stage, whereas a weakly convergent river with progressive wave characteristics exhibited peak flow velocity during high and low tide stage. Fourth, the strongly convergent river exhibited significantly higher sediment accretion (likely due to a single watershed runoff event) but exhibited significantly lower SSC during riparian wetland inundation than a weakly convergent tidal river.

[52] **Acknowledgments.** We thank Jackie Batson, Ed Schenk, Sara Ulrich, and Alice Besterman for field and laboratory assistance and Don and Mark Malloy and Christopher Vooris for access to docks on their property. Support was provided by the U.S. Geological Survey Mendenhall Research Fellowship Program, the U.S. Geological Survey National Research Program, and Aquatic Analysis and Consulting, LLC. Any use of trade, firm, or product names is for descriptive purposes only and does not imply endorsement by the U.S. Government.

References

Ahnert, F. (1960), Estuarine meanders in the Chesapeake Bay area, *Geogr. Rev.*, *50*(3), 390–401, doi:10.2307/212282.

Ashley, G. M. (1980), Channel morphology and sediment movement in a tidal river, Pitt river, British Columbia, *Earth Surf. Processes Landforms*, *5*(4), 347–368, doi:10.1002/esp.3760050406.

Baldwin, A. H. (2009), Vegetation and seed bank studies of salt-pulsed swamps of the Nanticoke River, Chesapeake Bay, in *Ecology of Tidal Freshwater Forested Wetlands of the Southeastern United States*, edited by W. H. Conner et al., pp. 139–160, Springer, New York.

Barendregt, A., D. Whigham, and A. Baldwin (2009), *Tidal Freshwater Wetlands*, Backhuys, Leiden.

Cahoon, D. R., J. C. Lynch, and R. M. Knaus (1996), Improved cryogenic coring device for sampling wetland soils, *J. Sediment. Res.*, *66*, 1025–1027.

Carle, M. V. (2011), Estimating wetland losses and gains in coastal North Carolina: 1994–2001, *Wetlands*, *31*(6), 1275–1285, doi:10.1007/s13157-011-0242-z.

Chen, M. S., S. Wartel, B. V. Eck, and D. V. Maldegem (2005), Suspended matter in the Scheldt estuary, *Hydrobiologia*, *540*(1), 79–104, doi:10.1007/s10750-004-7122-y.

Chen, Y., M. B. Collins, and C. E. L. Thompson (2011), Creek enlargement in a low-energy degrading saltmarsh in southern England, *Earth Surf. Processes Landforms*, *36*(6), 767–778, doi:10.1002/esp.2104.

Conner, W. H., T. W. Doyle, and K. W. Krauss (Eds.) (2009), *Tidal Freshwater Wetlands of the Southeastern United States*, Springer, Netherlands.

Cormier, N., K. W. Krauss, and W. H. Conner (2012), Periodicity in stem growth and litterfall in tidal freshwater forested wetlands: Influence of salinity and drought on nitrogen recycling, *Estuaries Coasts*, *36*(3), 533–546, doi:10.1007/s12237-012-9505-z.

Craft, C. B. (2012), Tidal freshwater forest accretion does not keep pace with sea level rise, *Global Change Biol.*, *18*(12), 3615–3623, doi:10.1111/gcb.12009.

Craft, C. B., J. Clough, J. Ehman, S. Joye, R. Park, S. Pennings, H. Guo, and M. Machmuller (2009), Forecasting the effects of accelerated sea-level rise on tidal marsh ecosystem services, *Front. Ecol. Environ.*, *7*(2), 73–78, doi:10.1890/070219.

Cronin, T. M. (Ed.) (2004), *Pocomoke Sound Sedimentary and Ecosystem History*, Open File Report 2004-1350, US Geological Survey, Reston, VA.

Dalrymple, R. W., and K. Choi (2007), Morphologic and facies trends through the fluvial-marine transition in tide-dominated depositional systems: A schematic framework for environmental and sequence-stratigraphic interpretation, *Earth Sci. Rev.*, *81*(3–4), 135–174, doi:10.1016/j.earscirev.2006.10.002.

Darke, A. K., and J. P. Megonigal (2003), Control of sediment deposition rates in two mid-Atlantic Coast tidal freshwater wetlands, *Estuarine Coastal Shelf Sci.*, *57*(1–2), 255–268, doi:10.1016/S0272-7714(02)00353-0.

Davies, G., and C. D. Woodroffe (2010), Tidal estuary width convergence: Theory and form in North Australian estuaries, *Earth Surf. Processes Landforms*, *35*(7), 737–749, doi:10.1002/esp.1864.

Downing, A., P. D. Thorne, and C. E. Vincent (1995), Backscattering from a suspension in the near-field of a piston transducer, *J. Acoust. Soc. Am.*, *97*(3), 1614–1620.

Eisma, D. (1986), Flocculation and de-flocculation of suspended matter in estuaries, *Neth. J. Sea Res.*, *20*(2/3), 183–199.

Ensign, S. H., M. W. Doyle, and M. F. Piehler (2013a), The effect of tide on the hydrology and morphology of a freshwater river, *Earth Surf. Processes Landforms*, *38*(6), 655–660, doi:10.1002/3sp.3392.

Ensign, S. H., C. R. Hupp, G. B. Noe, K. W. Krauss, and C. L. Stagg (2013b), Sediment accretion in tidal freshwater forests and oligohaline marshes of the Waccamaw and Savannah Rivers, U.S.A, *Estuaries Coasts*, doi:10.1007/s12237-013-9744-7.

Field, D. W., A. J. Reyer, P. V. Genovese, and B. D. Shearer (1991), Coastal wetlands of the United States, A special NOAA 20th anniversary Report, Strategic assessment Branch, Ocean Assessments Division, Office of Oceanography and Marine Assessments, National Ocean Service, National Oceanic and Atmospheric Administration and the US Fish and Wildlife Service, Washington, D. C.

Flick, E. F., D. B. Chadwick, J. Briscoe, and C. Harper (2012), "Flooding" versus "inundation", *Eos Trans. AGU*, *93*(38), 365–366, doi:10.1029/2012EO380009.

Friedrichs, C. T., and D. Aubrey (1988), Non-linear tidal distortion in shallow well-mixed estuaries: a synthesis, *Estuarine Coastal Shelf Sci.*, *27*(5), 521–545, doi:10.1016/0272-7714(88)90082-0.

Garofalo, D. (1980), The influence of wetland vegetation on tidal stream channel migration and morphology, *Estuaries*, *3*(4), 258–270, doi:10.2307/1352081.

Gartner, J. W. (2004), Estimating suspended solids concentrations from backscatter intensity measured by acoustic Doppler current profiler in San Francisco Bay, California, *Mar. Geol.*, *211*(3–4), 169–187, doi:10.1016/j.margeo.2004.07.001.

Gellis, A. C., C. R. Hupp, M. J. Pavich, J. M. Landwehr, W. S. L. Banks, B. E. Hubbard, M. J. Langland, J. C. Ritchie, and J. M. Reuter (2008), *Sources, Transport, and Storage of Sediment at Selected Sites in the Chesapeake Bay Watershed*, USGS Scientific Investigations Report 2008-5186, US Geological Survey, Reston, Va.

Geyer, W., J. Woodruff, and P. Traykovski (2001), Sediment transport and trapping in the Hudson River estuary, *Estuaries Coasts*, *24*(5), 670–679, doi:10.2307/1352875.

Guézennec, L., R. Lafite, J.-P. Dupont, R. Meyer, and D. Boust (1999), Hydrodynamics of suspended particulate matter in the tidal freshwater zone of a macrotidal estuary (the Seine Estuary, France), *Estuaries Coasts*, *22*(3), 717–727, doi:10.2307/1353058.

Hilgartner, W. B., and G. S. Brush (2006), Prehistoric habitat stability and post-settlement habitat change in a Chesapeake Bay freshwater tidal wetland, USA, *Holocene*, *16*(4), 479–494, doi:10.1191/0959683606hl938rp.

Hobbs, C. H., III (2004), Geological history of Chesapeake Bay, USA, *Quat. Sci. Rev.*, *23*, 641–661.

Hughes, Z. J. (2012), Tidal channels on tidal flats and marshes, in *Principles of Tidal Sedimentology*, edited by R. A. Davis and R. W. Dalrymple, pp. 269–300, Springer, Dordrecht, Netherlands.

Hupp, C. R., and D. E. Bazemore (1993), Temporal and spatial patterns of wetland sedimentation, West Tennessee, *J. Hydrol.*, *141*, 179–196.

John, S. J., and J. E. Pizzuto (1995), Accelerated sea level rise 2,000 years BP in the Delaware Bay: Stratigraphic evidence from the Leipsic River Valley, Delaware, U.S.A, *J. Coastal Res.*, *11*(3), 573–582.

Khan, H., and G. S. Brush (1994), Nutrient and metal accumulation in a freshwater tidal marsh, *Estuaries Coasts*, *17*(2), 345–360.

Krauss, K. W., J. A. Duberstein, T. W. Doyle, W. H. Conner, R. H. Day, L. W. Inabinette, and J. L. Whitbeck (2009), Site condition, structure, and growth of bald cypress along tidal/non-tidal salinity gradients, *Wetlands*, *29*, 505–519.

Kroes, D. E., C. R. Hupp, and G. B. Noe (2007), Sediment, nutrient, and vegetation trends along the tidal, forested Pocomoke River, Maryland, in *Ecology of Tidal Freshwater Forested Wetlands of the Southeastern United States*, edited by W. H. Conner et al., pp. 113–137, Springer, Dordrecht, Netherlands.

Lanzoni, S., and G. Seminara (2002), Long-term evolution and morphodynamic equilibrium of tidal channels, *J. Geophys. Res.*, *107*(C1), 3001, doi:10.1029/2000JC000468.

Leonard, L. A. (1997), Controls of sediment transport and deposition in an incised mainland marsh basin, southeastern North Carolina, *Wetlands*, *17*, 263–274.

Leonard, L. A., and D. J. Reed (2002), Hydrodynamics and sediment transport through tidal marsh canopies, *J. Coastal Res.*, *36*, 459–469.

Newell, W. L., and B. D. Dejong (2011), Cold-climate slope deposits and landscape modifications of the Mid-Atlantic Coastal Plain, Eastern USA, *Geol. Soc. London Spec. Publ.*, *354*(1), 259–276, doi:10.1144/SP354.17.

Noe, G. B., and C. R. Hupp (2005), Carbon, nitrogen, and phosphorus accumulation in floodplains of Atlantic Coastal Plain rivers, USA, *Ecol. Appl.*, *15*, 1178–1190.

Noe, G. B., and C. R. Hupp (2009), Retention of riverine sediment and nutrient loads by Coastal Plain floodplains, *Ecosystems*, *12*(5), 728–746.

Owens, J. P., and C. S. Denny (1979), *Upper Cenozoic deposits of the Central Delmarva Peninsula, Maryland and Delaware*, Professional Paper 1067-A, US Geological Survey, Reston, Va.

Pasternack, G. B. (2009), Hydrogeomorphology and sedimentation in tidal freshwater wetlands, in *Tidal Freshwater Wetlands*, edited by A. Barendregt, D. F. Whigham and A. H. Baldwin, pp. 31–40, Backhuys, Leiden.

Pethick, J. S. (1980), Velocity surges and asymmetry in tidal channels, *Estuarine Coastal Mar. Sci.*, *11*(3), 331–345, doi:10.1016/S0302-3524(80)80087-9.

Phillips, J. D. (1997), Human agency, Holocene sea level, and floodplain accretion in coastal plain rivers, *J. Coastal Res.*, *13*(3), 854–866.

Phillips, J. D., and M. C. Slattery (2006), Sediment storage, sea level, and sediment delivery to the ocean by coastal plain rivers, *Prog. Phys. Geogr.*, *30*(4), 513–530, doi:10.1191/0309133306pp494ra.

Phillips, J. D., and M. C. Slattery (2008), Antecedent alluvial morphology and sea-level controls on form-process transiiton zones in the lower Trinity River, Texas, *River Res. Appl.*, *24*, 293–309.

Pizzuto, J. E., and E. W. Rogers (1992), The Holocene history and stratigraphy of palustrine and estuarine wetland deposits of central Delaware, *J. Coastal Res.*, *8*(4), 854–867.

R Development Core Team (2009), *R: A Language and Environment for Statistical Computing*, R Foundation for Statistical Computing, Vienna, Austria. [Available at http://www.R-project.org.]

Reichel, G., and H. P. Nachtnebel (1994), Suspended sediment monitoring in a fluvial environment: Advantages and limitations applying an Acoustic Doppler Current Profiler, *Water Res.*, *28*(4), 751–761, doi:10.1016/0043-1354(94)90083-3.

Savenije, H. H. G. (2005), *Salinity and Tides in Alluvial Estuaries*, Elsevier Science Ltd, Amsterdam.

Schuchardt, B., and M. Schirmer (1990), Diatom frustules as natural tracers to determine the origin of suspended matter in the weser estuary, *Environ. Technol.*, *11*(9), 853–858, doi:10.1080/09593339009384933.

Schulkin, M., and H. W. Marsh (1962), Sound absorption in sea water, *J. Acoust. Soc. Am.*, *34*(6), 864–865.

Siegel, S., and N. J. Castellan (1988), *Non Parametric Statistics for the Behavioural Sciences*, McGraw Hill Int, New York.

Tambroni, N., M. B. Pittaluga, and G. Seminara (2005), Laboratory observations of the morphodynamic evolution of tidal channels and tidal inlets, *J. Geophys. Res.*, *110*, F04009, doi:10.1029/2004JF000243.

Thorne, P. D., P. J. Hardcastle, and R. L. Soulsby (1993), Analysis of acoustic measurements of suspended sediments, *J. Geophys. Res.*, *98*(C1), 899–910.

Urick, R. J. (1975), *Principles of Underwater Sound*, 2nd ed., McGraw Hill, New York.

Vermeer, M., and S. Rahmstorf (2009), Global sea level linked to global temperature, *Proc. Natl. Acad. Sci. U. S. A.*, *106*(51), 21,527–21,532, doi:10.1073/pnas.0907765106.

Vogelmann, J. E., T. L. Sohl, P. V. Campbell, and D. M. Shaw (1998), Regional land cover characterization using Landsat Thematic Mapper data and ancillary data sources, *Environ. Monit. Assess.*, *51*, 415–428, Third EMAP Research Symposium, Albany, NY, April 8-11, 1997.

Wall, G., E. Nystrom, and S. Litten (2008), Suspended sediment transport in the freshwater reach of the Hudson River Estuary in Eastern New York, *Estuaries Coasts*, *31*(3), 542–553, doi:10.1007/s12237-008-9050-y.

Williams, K., K. C. Ewel, R. P. Stumpf, F. E. Putz, and T. W. Workman (1999), Sea-level rise and coastal forest retreat on the West Coast of Florida, USA, *Ecology*, *80*(6), 2045–2063, doi:10.2307/176677.

Wright, L. D., J. M. Coleman, and B. G. Thom (1973), Processes of channel development in a high-tide-range environment: Cambridge Gulf-Ord River Delta, Western Australia, *J. Geol.*, *81*(1), 15–41.

Yankovsky, A. E., R. Torres, L. M. Torres-Garcia, and J. Kyungho (2012), Interaction of tidal and fluvial processes in the transition zone of the Santee River, SC, USA, *Estuaries Coasts*, *34*(6), 1500–1509.

Yanosky, T. M., C. R. Hupp, and C. T. Hackney (1995), Chloride concentrations in growth rings of Taxodium distichum in a saltwater-intruded estuary, *Ecol. Appl.*, *5*, 785–792.

Yarbro, L. A., P. R. Carlson, T. R. Fisher, J. P. Chanton, and W. M. Kemp (1983), A sediment budget for the Choptank River estuary in Maryland, U.S.A, *Estuarine Coastal Shelf Sci.*, *17*(5), 555–570, doi:10.1016/0272-7714(83)90007-0.